J. Biochem. 132, 471–482 (2002)

Analysis of the Conformational Change of Myosin during ATP Hydrolysis Using Fluorescence Resonance Energy Transfer[1]

Yoshiaki Mizukura and Shinsaku Maruta[2]

Department of Bioengineering, Faculty of Engineering, Soka University, Hachioji, Tokyo 192-8577

Received June 13, 2002; accepted July 11, 2002

In order to elucidate the molecular basis of energy transduction by myosin as a molecular motor, a fluorescent ribose-modified ATP analog 2′(3′)-*O*-[6-(*N*-(7-nitrobenz-2-oxa-1,3-diazol-4-yl)amino)hexanoyl]-ATP (NBD-ATP), was utilized to study the conformational change of the myosin motor domain during ATP hydrolysis using the fluorescence resonance energy transfer (FRET) method. The FRET efficiency from the fluorescent probe, BD- or AD-labeled at the reactive cysteine residues, SH1 (Cys 707) or SH2 (Cys697), respectively, to the NBD fluorophore in the ATP binding site was measured for several transient intermediates in the ATPase cycle. The FRET efficiency was greater than that using NBD-ADP. The FRETs for the myosin·ADP·AlF_4^- and myosin·ADP·BeFn ternary complexes, which mimic the M*·ADP·P_i state and M*·ATP state in the ATPase cycle, respectively, were similar to that of NBD-ATP. This suggests that both the SH1 and SH2 regions change their localized conformations to move closer to the ATPase site in the M*·ATP state and M·ADP·P_i state than in the M*·ADP state. Furthermore, we measured energy transfer from BD in the essential light chain to NBD in the active site. Assuming the efficiency at different states, myosin adopts a conformation such that the light chain moves closer to the active site by approximately 9 Å during the hydrolysis of ATP.**

Key words: energy transduction, fluorescent ATP analog, FRET, myosin.

It is well established that muscle contraction is driven by structural rearrangements within myosin during the ATPase cycle (*1–3*). Myosin is one of the main organizing proteins in muscle and contributes to muscle contraction by its interaction with actin. Although the driving force is obtained from the hydrolysis of ATP, it remains obscure how myosin transduces chemical energy from ATP to mechanical energy at the molecular level. Myosin hydrolyzes ATP through five steps in the ATPase cycle, and the following kinetic scheme of the myosin MgATPase cycle was developed based on observed changes in intrinsic tryptophan fluorescence (*4–10*), where M represents myosin and asterisks represent enhanced tryptophan fluorescence.

$$M + ATP \rightleftarrows M{\cdot}ATP \rightleftarrows M^*{\cdot}ATP \rightleftarrows M^{**}{\cdot}ADP{\cdot}P_i \rightleftarrows M^*{\cdot}ADP{\cdot}P_i \rightleftarrows M + ADP + P_i$$

Scheme 1

In this reaction myosin first forms a collision complex with ATP followed by isomerization to the M*·ATP complex, which results in the first level of fluorescence enhancement (*). During the rapid reversible process of ATP hydrolysis, a structural change induces an additional fluorescence enhancement (**). The fluorescence then decreases back to the first level of enhancement (*) following ATP hydrolysis, which is thought to correspond to the rate-limiting structural change resulting in phosphate release. The phosphate release step shifts myosin from a weak to a strong binding conformation in the interaction with actin and is the step believed to be associated with force generation during muscle contraction. The enhancement of tryptophan fluorescence reflects the conformations of the intermediate compounds. Thus, examining the conformational changes that result in alterations in intrinsic tryptophan fluorescence may yield important insights into the structural properties of the myosin MgATPase cycle. Investigation of the conformations of the myosin head in intermediate states is, therefore, significant for understanding the mechanism of myosin motility. However, intermediates in the ATPase cycle have only a limited lifetime, and thus it is difficult to recognize conformational changes of the myosin head during continuous ATPase cycling. Consequently, stable analogs myosin-ADP-fluorometals corresponding to these interme-

[1]This work was supported by Grants-in-Aid for Scientific Research C (11680667) from the Ministry of Education, Science, Sports and Culture of Japan.

[2]To whome correspondence should be addressed. Tel: +81-426-91-9443, Fax: +81-426-91-9312, E-mail: shinsaku@t.soka.ac.jp

Abbreviations: AD, 6-acryloyl-2-dimethylaminonaphthalene; AlF_4^-, aluminum fluoride; BD, 6-bromoacetyl-2-dimethylaminonaphthalene; BD-A1 or BD-A2, S1 (A1) or S1 (A2) labeled by BD; BeF_n, beryllium fluoride; DMF, *N,N-dimethylformamide*; DTT, dithiothreitol; ELC, essential (alkali) light chain; FDNB, 2,4-dinitro-1-fluorobenzene; FEDA-ATP, 2′(3′)-*O*-[*N*-[2-[3-(5-fluoresceinyl)thioureico]ethyl] carbamoyl]adenosine 5′-triphosphate; FRET, fluorescence resonance energy transfer; GaF_n, gallium fluoride; HEPES, 2-[4-(2-hydroxyethyl)-1-piperazinyl]ethanesulfonic acid; HMM, heavy meromyosin; MgF_n, magnesium fluoride; MOPS, 3-(*N*-morpholino)propanesulfonic acid; NBD-ATP, 2′(3′)-*O*-[6-(*N*-(7-nitrobenz-2-oxa-1,3-diazol-4-yl)amino)hexanoyl]-ATP; PIPES, piperazine-1,4-bis(2-ethanesulfonic acid); RLC, regulatory light chain; ScF_n, scandium fluoride; S1, myosin subfragment-1; S1 (A1) or S1 (A2), myosin subfragment-1 carrying alkali light chain A1 or A2; SDS-PAGE, sodium dodecyl sulfate polyacrylamide gel electrophoresis; TLC, thin layer chromatography.

diates are valuable tools.

Goodno (*11*) was the first to demonstrate that in the presence of MgADP, orthovanadate (V_i) could form a stable ternary complex with myosin, corresponding to a 1:1:1 ternary complex designated M·ADP·V_i, which mimics the steady-state intermediate, M**·ADP·P_i of the ATPase cycle. Furthermore, it was shown that the phosphate analogs of fluorometals, aluminum fluoride (AlF_4^-) (*12, 13*), beryllium fluoride (BeF_n) (*12–14*), scandium fluoride (ScF_n) (*15*), gallium fluoride (GaF_n) (*16*) and magnesium fluoride (MgF_n) (*17, 18*), also form stable ternary complexes of M·ADP·fluorometal. Differences exist in their interactions with actin, and each complex may resemble a distinct reaction intermediate of the myosin ATPase cycle (*12*). Structural studies have demonstrated differences in the converter region when comparing the crystal structure of the myosin head from *Dictyostelium discoideum* myosin II in each phosphate analog (*19, 20*). Maruta *et al.* (*12, 16, 17*) proposed that the possible alignment of the ternary complexes in the ATPase cycle is as follows:

$$\text{M}^*\cdot\text{ATP} \underset{\text{*BeF}_n}{\rightleftharpoons} \text{M}^{**}\cdot\text{ADP}\cdot\text{P}_i \underset{\text{MgF}_n,\ \text{AlF}_4^-,\ (\text{ScF}_n)}{\rightleftharpoons} \text{M}^*\cdot\text{ADP} + \text{P}_i$$

Scheme 2

where *BeF_n and **BeF_n indicate different species of MgF_n depending on the number of F bound to Be.

The crystal structure of skeletal myosin subfragment-1 has been elucidated (*19–21*), and therefore the conformational change of the myosin head during the ATPase cycle can be investigated at the molecular level. Studies using electron microscopy and X-ray scattering have shown that the conformation of the myosin head changes dramatically during ATP hydrolysis (*22–25*). A striking feature of the S1 structure is a long helix spanning 85 Å that is stabilized by interactions with the myosin light chains (*21*). It has been proposed that this light chain domain acts as a semi-rigid "lever arm" to amplify and transmit conformational changes in the ATP and actin binding sites of S1 (*19, 26–31*). To account for the currently measured step size for myosin, ~40–110 Å (*32–34*), a substantial swing of at least 60°C is required (*35*). Many lines of experimental evidence support the involvement of this helix in the force generation (*20, 25, 27, 29, 36–41*), although no direct proof of its movement during muscular contraction has yet emerged.

The myosin head has two highly reactive cysteine residues, Cys 707 (SH1) and Cys 697 (SH2), which have been documented previously (*19, 27–31, 42–52*). SH1 and SH2 are located on two different helices in the C-terminal segment of the S1 catalytic domain and are separated from one another by 19 Å (*21*). Previous biochemical studies have suggested that this helix has a role in transducing signals from the actin or ATP binding site to the converter region and lever arm (*27, 29–30, 45–52*), and recent reports have led to the conclusion that the fulcrum point for the swinging motion of the lever arm is in the vicinity of the SH1-SH2 region (*19, 28, 31*). In particular, Gly 699 (close to SH2) and Gly 710 (close to SH1) have been proposed to act as pivot points or flexible hinges for such motion (*31, 37, 53*). This suggests the importance of motion in the SH1–SH2 region for the force generation cycle of myosin.

In the present study, we used the fluorescent ATP analog 2′(3′)-*O*-[6-(*N*-(7-nitrobenz-2-oxa-1,3-diazol-4-yl)amino)hexanoyl]-ATP (NBD-ATP) for fluorescence resonance energy transfer (FRET) to study conformational changes of the myosin head in the ATPase cycle that may be directly related to energy transduction. FRET from SH1 or SH2 (labeled by fluorescent probes BD and AD, respectively) to the active site where NBD-ADP binds was measured to monitor spatial distance changes between the two functional sites. FRET is a useful strategy to investigate the details of a conformational change between two points under physiological conditions (*54, 55*). Furthermore, we measured energy transfer from the essential light chain to the active site to detect directly the bending of the myosin head, which would support the lever arm hypothesis.

MATERIALS AND METHODS

Chemicals—NBD acid, AD, and BD were purchased from Molecular Probes (Eugene, OR). Carbonyldiimidazole was from Sigma Chemical (St. Louis, MO). $BeSO_4$, $AlCl_3$, NaF, and ATP were from Wako Pure Chemical Industries (Osaka).

Protein Preparation—Skeletal muscle myosin was prepared from chicken breast muscle following the methods of Perry (*56*). S1 was then obtained from myosin by digestion with α-chymotrypsin as described by Weeds and Taylor (*57*). The A1 and A2 isoforms of ELC were separated by high performance liquid chromatography (HPLC) using a DEAE-5PW column on a linear NaCl gradient (0–225 mM) in 50 mM MOPS (pH 7.0) at a flow rate of 1 ml/min. Protein concentration was determined by the biuret reaction (*58*) and Bradford assay (for protein concentrations < 1 mg/ml) (*59*).

Synthesis of 2′(3′)-O-[6-(N-(7-Nitrobenz-2-oxa-1,3-diazol-4-yl)amino)hexanoyl]-ATP (NBD-ATP)—Coupling of ATP and 6-(*N*-(7-nitrobenz-2-oxa-1,3-diazol-4-yl)amino)hexanoic acid (NBD acid) was performed according to the method reported recently by us (*60*). NBD acid (68 μmol) and carbonyldiimidazole (204 μmol) were stirred for 30 min at room temperature in 0.48 ml of dry *N,N*-dimethylformamide (DMF). ATP (34 μmol) was dissolved in 0.51 ml of water and added dropwise to the reaction mixture. The coupling reaction was allowed to proceed for 48 h at room temperature with continuous stirring. The reaction mixture was evaporated to dryness and the residue dissolved in 1 ml of 0.1% TFA. The product was purified by HPLC using an RP-C18 column. Elution was performed on a linear acetonitrile gradient (0 to 90%) in 0.1% TFA at a flow rate of 1 ml/min. The elution profile was monitored by absorbance at 275 nm. Three major peaks were obtained. The first peak that eluted was unreacted ATP, and third was the unreacted NBD acid. The second peak contained NBD-ATP. The fractions were collected and lyophilized. The purity of the product was analyzed by thin layer chromatography (TLC) on silica gel plates (Silica Gel-70 F254, Wako) using 1-butanol/acetic acid/H_2O (5:1:3, by volume) as the developing solvent. A single spot of NBD-ATP was observed, and the R_f value was 0.35.

Fluorescence Spectroscopy—Steady state fluorescence was measured using a HITACHI RF-2500 fluorescence spectrophotometer. NBD-ATP fluorescence was measured at 535 nm with excitement at 475 nm. BD and AD fluorescence emission spectra were measured with excitation at 390 nm and collection of the emitted fluorescence at 405–

610 nm.

Measurement of ATPase Activity—The Ca^{2+}- and K^+-ATPase activities were measured at 25°C in a reaction mixture containing 1 μM S1 (or labeled S1), 0.5 M KCl, 50 mM Tris-HCl (pH 7.5), 5 mM $CaCl_2$ (or EDTA), and 2 mM ATP. The reaction was stopped by the addition of 10% trichloroacetic acid, and the released P_i was measured by the method of Youngburg and Youngburg (*61*).

Measurement of Sliding Velocity of F-Actin on Myosin Using NBD-ATP—Skeletal muscle myosin heavy meromyosin (HMM, 80 μg/ml) in high salt solution [0.5 M KCl, 20 mM PIPES (pH 7.5), 2 mM $MgCl_2$, and 0.1 mM dithiothreitol (DTT)] was perfused into a flow cell made of a nitrocellulose-coated glass coverslip. After 5 min, the flow cell was rinsed with the high salt solution including 1 mg/ml BSA, and then left for 5 min, and, finally, 10 nM F-actin filaments labeled with rhodamine-conjugated phalloidin (Molecular Probe) in motility buffer [25 mM KCl, 25 mM imidazole (pH 7.5), 2 mM ATP, 4 mM $MgCl_2$, 1 mM EGTA, 10 mM DTT, 1 mg/ml BSA, 0.2% methyl cellulose, 1% β-mercaptoethanol, 4.5 mg/ml glucose, 210 μg/ml glucose oxidase, and 35 μg/ml catalase] were perfused into the flow cell. The above treatments were performed at 0°C. The flow cell was then equilibrated for 5 min between the temperature-controlled slide carrier and temperature-jacketed objective of an inverted-microscope. Methylcellulose was required to observe the F-actin sliding on both isoform preparations. Fluorescent F-actin filaments were examined with an inverted microscope (Axiovert 35; Zeiss Neofluoar × 100 objective [N.A. 1.3]) and SIT camera (C2400-08; Hamamatsu Photonics, Hamamatsu), and recorded on S-VHS videotape (AG7355; Panasonic, Osaka). Selected video frames were digitized with a frame grabber (LG-3; Scion, Frederick, MD) and NIH image analysis software. The sliding velocity of fluorescent F-actin was calculated by measuring the displacement of the filament between successive video frames using a tracking program included within the NIH image analysis software.

Fluorescence Labeling of Cys 707 (SH1) and Cys 697 (SH2) with AD and BD—S1 was incubated with a 4-fold (AD) or 3-fold (BD) molar excess of the reagent over S1 according to Hiratsuka (*62*). Fluorescence labeling was performed at 7°C for 20 min (AD) or 7 min (BD) in 30 mM KCl, 25 mM HEPES (pH 8.0), 2 mM $MgCl_2$, and 0.3% DMF in the dark. The reaction mixture contained 0.3% DMF because both AD and BD are scarcely soluble in water. The addition of 0.3% DMF had no effect on the Mg^{2+}-, Ca^{2+}-, and K^+-ATPase activity of S1. The reaction was stopped by the addition of 2 mM DTT. The reaction products were passed through a Sephadex G-50 spin column equilibrated with 30 mM KCl and 25 mM HEPES (pH 8.0) to remove excess unreacted reagent.

Fluorescence Labeling of Cys 177 (Cys 136) in Essential Light Chain A1 (A2) with BD—In order to avoid labeling Cys 707 (SH1), this residue was preblocked with 2,4-dinitro-1-fluorobenzene (FDNB) as described previously (*48*). The separated S1 was incubated with FDNB at 0°C for 60 min in 30 mM KCl, 25 mM HEPES (pH 8.0), and 2 mM $MgCl_2$. After removal of the excess reagent by centrifugal gel filtration on a Sephadex G-50 column, the only reactive thiol in the absence of nucleotide was Cys 177 or Cys 136 on light chain A1 or A2, respectively; this residue was modified with BD (Molecular Probes) using a 4-fold molar excess of reagent over S1 for 15 min (A1) or 7 min (A2) on ice. The reaction was stopped, and the dinitrobenzene group (as a protector of SH1) was removed by adding 20 mM DTT and leaving the protein overnight on ice. The excess dye and DTT were removed by centrifugal gel filtration on a Sephadex G-50 column equilibrated with and then dialyzed against 30 mM KCl, 25 mM HEPES (pH 8.0), and 0.5 mM DTT.

Quantification of AD- and BD-Bound S1—The stoichiometry of fluorophore/S1 was determined from the absorption spectrum in 30 mM KCl and 25 mM HEPES (pH 8.0) using extinction coefficients of 12,000 $M^{-1}\cdot cm^{-1}$ at 382 nm for AD-S1 and 12,300 $M^{-1}\cdot cm^{-1}$ at 392 nm for BD-S1 (*62*). The amount of BD bound to A1 and A2 was assessed by the densitometric profile from SDS polyacrylamide gel electrophoresis (SDS-PAGE).

Fluorescence Resonance Energy Transfer Measurements—FRET was used to measure the distance between the donor fluorophores, BD, and acceptor fluorophores, NBD-labeled nucleotides, according to the Förster energy transfer theory (*54*). The efficiency of FRET was calculated from the decrease in the donor emission intensity upon acceptor excitation using the following equation,

$$E = 1 - F_{DA}/F_D \quad (1)$$

where F_{DA} is the fluorescence intensity from the emission spectrum of the donor in the presence of acceptor, corrected by subtracting the inner filter effect, and F_D is the fluorescence intensity from the emission spectrum of the donor.

The distance (r) between the donor and acceptor fluorophores can be calculated with Eq. 2,

$$r = R_0 (E^{-1} - 1)^{1/6} \text{ (Å)} \quad (2)$$

where R_0 is the Förster critical distance at which energy transfer is equal to 50%. The distance R_0 is calculated from Eq. 3,

$$R_0 = 9.79 \times 10^3 (K^2 J Q_D n^{-4})^{1/6} \text{ (Å)} \quad (3)$$

where K^2 is the orientation factor assuming free rotation of the donor and acceptor fluorophore. A K value of 2/3 for the NBD fluorophore of NBD-ADP trapped in the ATPase site by fluorometals was used, because the fluorophore is linked to ribose through a long spacer (amino hexanoyl), and so is thought to exist sufficiently outside the ATP binding cleft to rotate relatively freely; Q_D is the quantum yield of the donor, 0.18 and 0.11 for AD (*63*) and BD (the quantum yield of BD determined using that of AD in H_2O as the standard sample), respectively; n is the refractive index of the buffer (1.4); and J is the spectral overlap integral in $cm^3\cdot M^{-1}$ given by Eq. 4.

$$J = \Sigma F_D(\lambda)\varepsilon_A(\lambda)\lambda^4 d\lambda \ (cm^3\cdot M^{-1}) \quad (4)$$

In this equation $F_D(\lambda)$ is the normalized total integrated intensity of the unquenched donor group and ε_A is the extinction coefficient of the acceptor in $M^{-1}\cdot cm^{-1}$. J was numerically integrated at 1-nm intervals and determined in all nucleotide states studied, where λ is the wavelength in centimeters.

RESULTS

Specific Modification of SH1 and SH2—The structure of

the fluorophore moiety of AD and BD, the 6-acyl-2-dimethyleaminonaphthalene group, is the same as that of the noncovalent probe prodan (*61*). Therefore, these reagents can be expected to show fluorescence that is as extremely sensitive to solvent polarity as prodan. A recent study has shown that SH1 and SH2 are selectively labeled by the fluorescent probes BD and AD, respectively, whose emission spectra overlap with the excitation spectrum of NBD-ATP (*62*). Figure 1 shows the time course of labeling of SH2 and SH1 by AD (Fig. 1A) and BD (Fig. 1B), respectively, as carried out at 7°C with a 4- fold (AD) or 3-fold molar excess (BD) of dye over S1 in the dark. This was followed by measuring the amounts of labeled thiol groups. The amounts of labeled thiol groups were determined using the extinction coefficients for AD (12,000 $M^{-1}\cdot cm^{-1}$) and BD (12,300 $M^{-1}\cdot cm^{-1}$) as shown previously by Hiratsuka (*62*). Labeling of SH2 was relatively rapid for the first 30 min and much slower thereafter. On the other hand, the rate of the labeling by BD was faster than labeling by AD. The exact incorporated amounts, 0.85 for AD and 0.82 for BD (mol/mol ·S1), were estimated by extrapolation of the slow labeling to zero time.

It is well established that modifications of SH1 and SH2 affect ATPase activity. Thus, the status of the reaction was confirmed by measuring of Ca^{2+}-, or K^+-ATPase activity (Fig. 1, A and B, inset, respectively). For the labeling of SH2 with AD, the K^+-ATPase activity decreased linearly to 40% of the original value as the number of labeled thiol groups increased. On the contrary, the Ca^{2+}-ATPase was not affected by labeling with AD. For the labeling of SH1 with BD, the K^+-ATPase activity showed a similar change to that of AD, while the Ca^{2+}-ATPase activity was increased linearly in contrast to the change in K^+-ATPase activity.

SDS-PAGE analysis of labeled S1 revealed that the fluorescence of AD or BD is observed predominantly in the 95-kDa (heavy) chain and its 20-kDa tryptic fragments that contain SH1 and SH2 (Fig. 2, A and B), but that the light chains are also slightly labeled with BD. Densitometric analysis of the gel showed the percentage of incorporated BD labeling SH1 and the two light chains to be 76 and 24%, respectively.

Fluorescent Labeling of ELC—Prior to the specific labeling of the ELC of S1, isoforms of the ELC (A1 and A2) were separated from intact S1 by HPLC using a DEAE anion-exchange column as described previously. As shown in Fig. 3, four major peaks were eluted with a NaCl gradient of 0–225 mM. Peaks A and B eluting at 59–67 min were identified as the A1 isoforms, and peaks C and D eluting at 69–76 min were identified as the A2 isoforms by SDS-PAGE (data not shown). In order to label Cys 177 (A1) and Cys 136 (A2) in the ELC specifically with BD, the first reactive cysteine residue SH1 (Cys 707) in the heavy chain was blocked with FDNB. S1 and FDNB were incubated in 30 mM KCl and 25 mM HEPES (pH 8.0) on ice. The reaction was monitored by the alteration in the ATPase activity accompanying the modification of SH1 (Fig. 4). Labeling with FDNB of both S1 (A1) and (A2) resulted in a 300% increase in the Ca^{2+}-ATPase activity and an approximate 10% decrease in the K^+-ATPase activity. The results indicate that SH1 is completely blocked by FDNB. Subsequently, the light chains A1 or A2 of dinitrophenylated (DNP)-S1 were labeled with BD under the same conditions as used to label of SH1 with BD. The DNP bound to SH1 as a blocking group was removed by incubating with a reducing reagent (DTT). The deblocking reaction was confirmed by the recovery of the ATPase (Fig. 5). As shown in Fig. 6, the rate of labeling of A2 by BD was somewhat faster than that of A1. Protection of SH1 was confirmed by electrophoresis (Fig. 7). Both A1 and A2 were predominantly labeled by BD (71% for A1 and 87% for A2), but the heavy chain was also slightly labeled by BD (29–13%) due to incomplete blocking by FDNB. The S1 labeled by BD at the ELC (0.7–0.8 mol·BD/mol·S1) was used for all FRET experiments.

Conformational Change in the SH1 and SH2 Region during the ATPase Cycle—The fluorescence excitation spectrum of NBD-ATP overlapped the emission spectra of AD and BD, as shown in Fig. 8. Therefore, efficient FRET is expected between the two fluorophores. The J values under the different nucleotide states were calculated from the spectral overlap of AD or BD and NBD-ATP by numerical

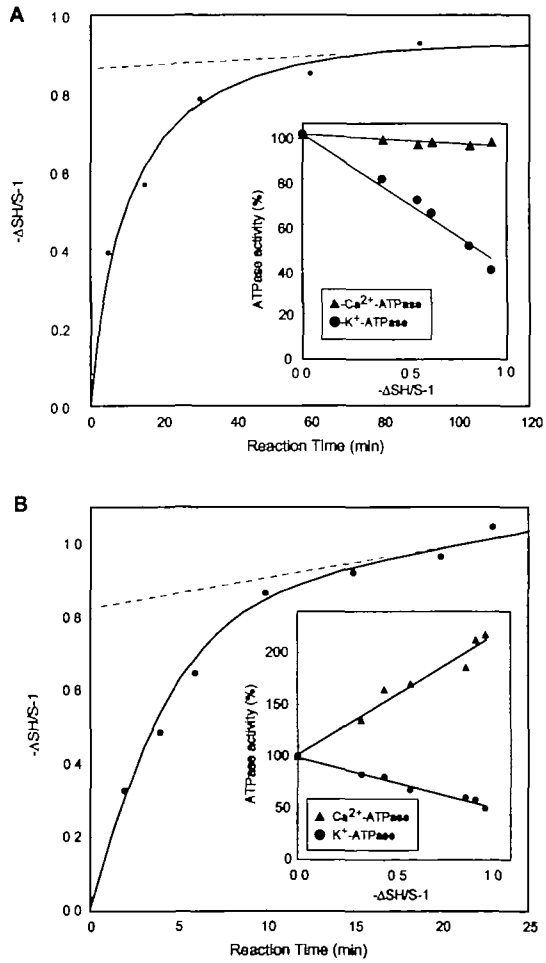

Fig. 1. **Time course of thiol groups labeling.** S1 was modified with a 4- or 3-fold molar excess of AD (A) or BD (B) over S1, respectively, at 7°C in the dark. The proportion of labeled thiol groups was determined by the extinction coefficients for AD (12,000 $M^{-1}\cdot cm^{-1}$) and BD (12,300 $M^{-1}\cdot cm^{-1}$). Buffer conditions were as follows: 30 mM KCl, 25 mM HEPES (pH 8.0), 2 mM $MgCl_2$, and 0.3% DMF. Both reactions were stopped by the addition of 2 mM DTT. Inset shows the relationship between ATPase activity and the proportion of labeled thiol groups. Labeled S1 (1 μM) was preincubated with 1 mM ATP, 0.5 M KCl, 50 mM Tris-HCl (pH 7.5), and 5 mM $CaCl_2$ (or EDTA) at 25°C.

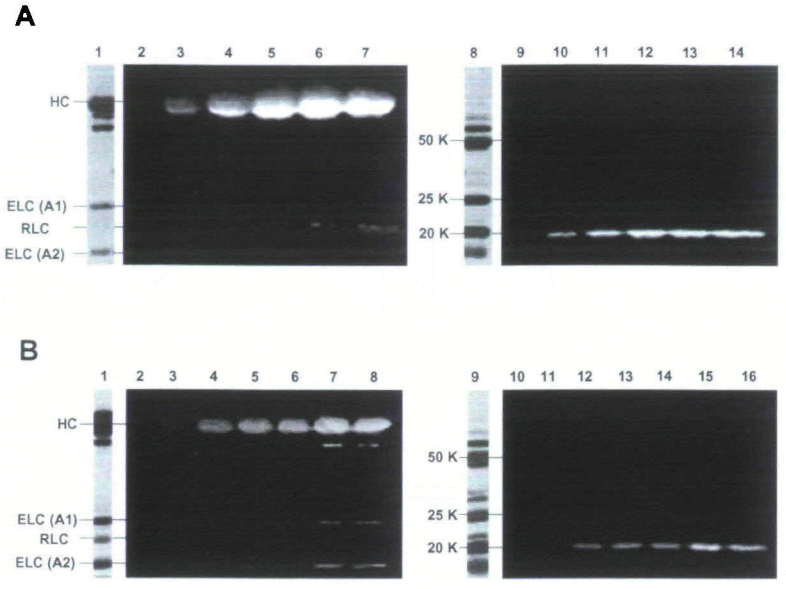

Fig. 2. **Specific labeling of the S1 heavy chain with AD or BD.** Labeled S1 was subjected to SDS-PAGE in 15% acrylamide gels. HC, heavy chain; LC, light chain. (A) S1 was labeled with AD (lanes 1–7), and then digested with 1/100 (w/w) trypsin for 30 min at 25°C (lanes 8–14); lanes 1 and 8, S1 labeled with AD of its tryptic fragment stained with Coomassie Brilliant Blue; lanes 2, 3, 4, 5, 6, and 7, fluorescence of AD-labeled S1 under UV irradiation at 480 nm, modification time of S1 with AD = 0, 5, 15, 30, 60, and 90 min, respectively; lanes 9, 10, 11, 12, 13, and 14, tryptic digests of the samples corresponding to lanes 2–7. (B) S1 was labeled with BD (lanes 1–8), and then digested with trypsin under the same conditions as for AD (lanes 10–16); lanes 1 and 9, S1 labeled with BD of its tryptic fragment stained with Coomassie Brilliant Blue; lanes 2, 3, 4, 5, 6, 7, and 8, fluorescence of BD-labeled S1 under UV irradiation at 480 nm, modification time of S1 with BD = 0, 2, 4, 6, 10, 15, and 20 min, respectively; lanes 10, 11, 12, 13, 14, 15, and 16, tryptic digests of the samples corresponding to lanes 2–8.

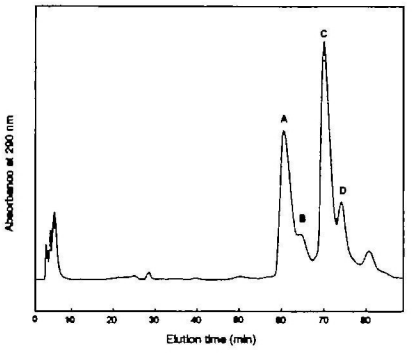

Fig. 3. **Separation of intact S1 by HPLC using a DEAE anion-exchange column.** 10 mg/ml S1 (850 μl) was applied on a DEAE-5PW column equilibrated with 50 mM MOPS (pH 7.0) using a micro injector (sample loop; 1 ml). Fractions were eluted with a linear NaCl gradient of 0–225 mM for 90 min at a flow rate of 1 ml/min.

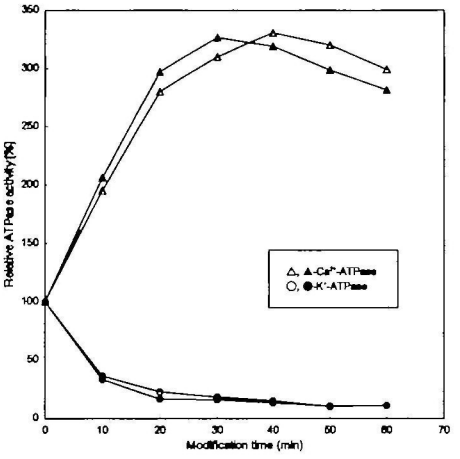

Fig. 4. **Blocking of SH1 with 2,4-dinitro-1-fluorobenzene.** Modification with 2,4-dinitro-1-fluorobenzene was monitored by changes in Ca^{2+}- and K^+-ATPase activity. S1 (A1) and S1 (A2) were blocked with a 5-fold molar excess of 2,4-dinitro-1-fluorobenzene over protein at 0°C in 30 mM KCl and 25 mM HEPES (pH 8.0); S1 (A1), open circles and triangles; S1 (A2), solid circles and triangles.

integration in each component (Eq. 4, see "MATERIALS AND METHODS" for the calculation). In a preliminary FRET study, the time course of the fluorescence change for BD-S1 accompanied by ATP hydrolysis was measured (Fig. 9). The addition of NBD-ATP to BD-S1 resulted in a 28% decrease in the original fluorescence intensity of BD. This decrease was larger than when regular ATP was added to BD-S1. The difference in fluorescence intensity between the BD-S1/NBD-ATP and BD-S1/regular ATP indicates the apparent energy transfer. After complete hydrolysis of NBD-ATP, the fluorescence intensity was not recovered completely upon the addition of excess ATP. This incomplete recovery can be explained by the inner filter effect of NBD-ATP (Fig. 9).

For FRET measurements, a 5-fold molar excess of NBD-ATP was added to AD- or BD-labeled-S1 to occupy the active site of S1 completely. To compensate for the inner filter effect of NBD-ATP, the ATPase site was blocked by ADP·BeF_n, which binds strongly to the ATPase site and forms a stable ternary complex with S1, and then the same concentration of NBD-ATP (3 μM) was added. The efficiencies of energy transfer from AD at SH2 to NBD in the active site were estimated from the change in the donor emission spectrum at 500 nm under several transient states in myosin ATPase (Fig. 10A). As a control, the spectrum of AD-S1·ADP·AlF_4^- or AD-S1·ADP·BeF_n was used. Efficiency derived from the difference spectrum from control was highest for the NBD-ADP·BeF_n complex, which mimics the M^*·ATP state (12.8%). The efficiencies for other complexes were 7.4% for NBD-ADP·AlF_4^-, 5.9% for NBD-ATP and 4.0% for NBD-ADP (Table I). On the other hand, the efficiency of energy transfer for BD-S1 was much higher than that of AD-S1 (Fig. 10, A and B). Efficiencies were 45.8% for NBD-ADP·BeF_n, 36.2% for NBD-ATP, 32.6% for NBD-ADP, and 32.7% for NBD-ADP·AlF_4^-.

R_0, the distance when the efficiency of energy transfer is 50%, was about 34 Å for AD-S1·NBD-ATP, and 31 Å for BD-S1·NBD-ATP, calculated from Eq. 3. The distances were 54.3, 58.4, 47.2, and 52.1 Å for AD-S1·NBD-ADP, AD-S1·NBD-ATP, AD-S1·NBD-ADP·BeF_n, and AD-S1·NBD-

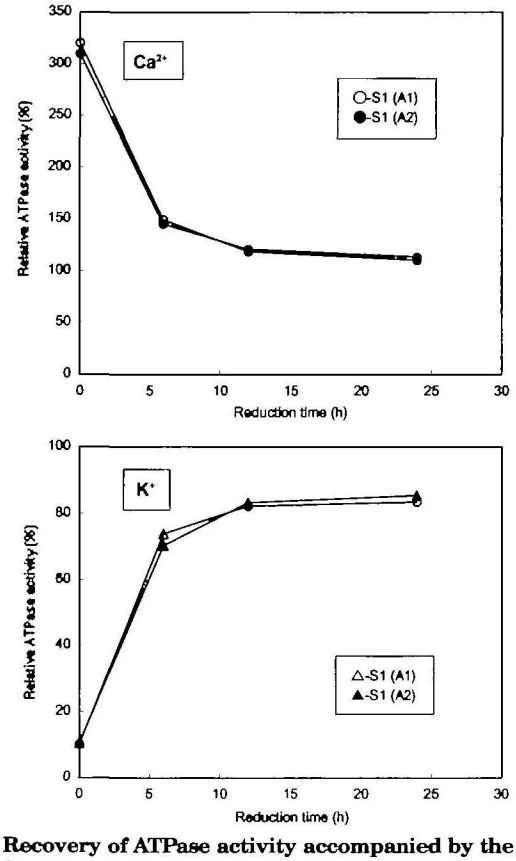

Fig. 5. **Recovery of ATPase activity accompanied by the reduction of FDNB.** At time zero, 20 mM DTT was added to remove FDNB (the protector for SH1). An ATPase activity of 100% indicates the activity of S1 before modification by FDNB. Measurement of ATPase activity was performed under the following conditions: 1 μM S-1, 0.5 mM ATP or NBD-ATP, 0.5 M KCl, 50 mM Tris-HCl, pH 7.5, at 25°C including 5 mM of $CaCl_2$ or EDTA. (Upper) Time course of Ca^{2+}-ATPase activity. (Lower) Time course of K^+-ATPase activity; open circles and triangles for S1 (A1); solid circles and triangles for S1 (A2).

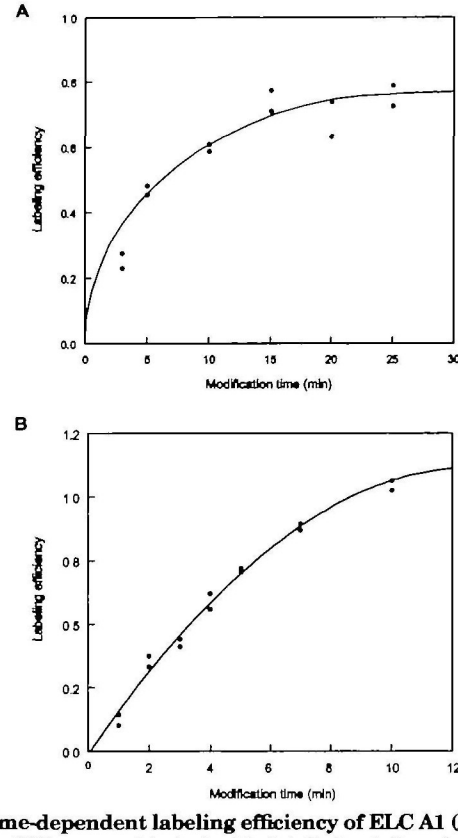

Fig. 6. **Time-dependent labeling efficiency of ELC A1 (A) and A2 (B).** After SH1 was preblocked with 2,4-dinitro-1-fluorobenzene, S1 was modified with a 4-fold molar excess of BD over S1 at 7°C in the dark. Buffer conditions were as follows; 30 mM KCl, 25 mM HEPES (pH 8.0), 2 mM $MgCl_2$, and 0.3% DMF. The reaction was stopped by the addition of 20 mM DTT, and the modified S1 was left overnight on ice to remove the dinitrobenzene group (the protector for SH1). Excess dye and DTT were removed by centrifugal gel filtration and dialysis.

ADP·AlF_4^-, respectively, and 35.3, 34.5, 32.2, and 35.1 Å for BD-S1·NBD-ADP, BD-S1·NBD-ATP, BD-S1·NBD-ADP·BeF_n, and BD-S1·NBD-ADP·AlF_4^-, respectively (Table I). These results suggest that both AD and BD change their localized conformation to be closest in the MgADP·BeF_n complexes, which mimic the M^*·ATP state.

Detection of the Conformational Changes Supporting Bending of the Myosin Head—To detect a conformational change, such as bending of the myosin head, which would induce an alteration in the relative distance between the regulatory domain and motor domain, we assayed FRET from BD-labeled ELC to NBD-ATP in the active site (Fig. 11). FRET measurements were performed as described above. For BD-A1, the values of J were determined by comparing the fluorescence emission spectra of donor in the absence of acceptor, and the excitation spectra of acceptor in the absence of donor under the same conditions, yielding an R_0 of 30.6–30.8 Å. The calculated energy transfer efficiencies were 8.2% for BD-A1·NBD-ADP, 14.6% for BD-A1·NBD-ATP, 22.6% for the BD-A1·NBD-ADP·BeF_n ternary complex and 24.7% for the BD-A1·NBD-ADP·AlF_4^- ternary complex, which convert to distances between Cys 177 of A1 and the active site of 46.1, 41.1, 37.6, and 37.1 Å, respectively (Fig. 11A and Table II). For BD-A2, FRET

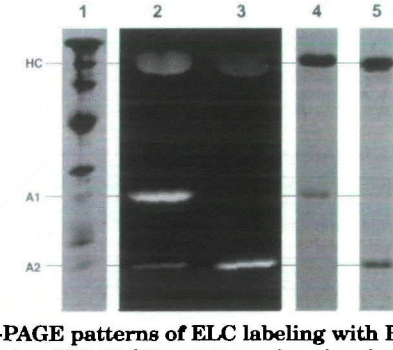

Fig. 7. **SDS-PAGE patterns of ELC labeling with BD.** Labeled S1 was subjected to SDS-PAGE in 15% acrylamide gels. Lane 1, molecular weight markers, 200, 95, 66, 45, 30, 20, and 17 kDa from top to bottom; lanes 2 and 3, fluorescence of BD under UV irradiation at 480 nm; lanes 4 and 5, corresponding bands stained with Coomassie Brilliant Blue.

measurements were performed under the same conditions (Fig. 11B). The values of R_0, 30.5–30.8 Å, were predicted from the values of J. The calculated energy transfer efficiencies were 7.3% for BD-A2·NBD-ADP, 6.3% for BD-A2·NBD-ATP, 20.9% for the BD-A2·NBD-ADP·BeF_n ternary complex, and 14.3% for the BD-A2·NBD-ADP·AlF_4^-

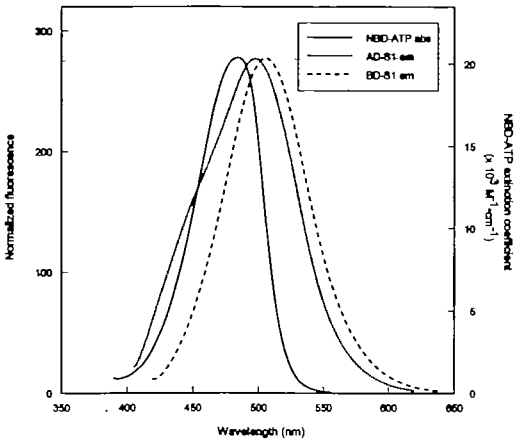

Fig. 8. **Spectral overlap of NBD-ATP absorption with AD and BD fluorescence.** The absorption spectrum of NBD-ATP (fluorescence acceptor; solid line) and the normalized fluorescence emission spectra of AD- and BD-S1 (fluorescence donor; dotted line, dashed line) were plotted. The spectra were measured in 20 mM Tris-HCl, (pH 7.5).

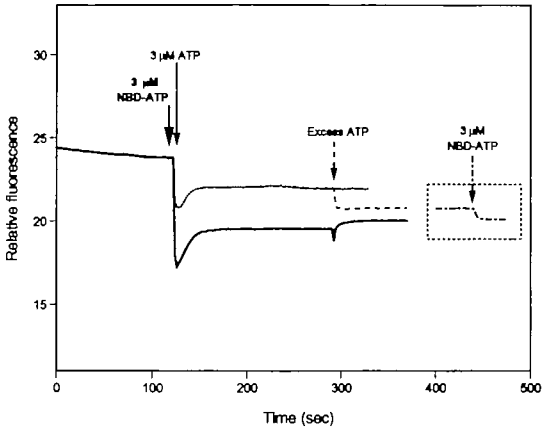

Fig. 9. **Fluorescence transients observed upon the addition of NBD-ATP or ATP.** The reaction was monitored by BD fluorescence (500 nm) excited at 390 nm. To BD-S1 (1 μM), 3 μM NBD-ATP (bold line) or 3 μM ATP (dotted line) or excess ATP (dashed line) was added at 25°C. Square dashed line; 1 μM BD-S1 was preincubated with 0.1 mM ADP and 1 mM BeF_n for 1 h, and then 3 μM NBD-ATP was added (dashed line). Buffer conditions were as follows: 120 mM NaCl, 30 mM Tris-HCl (pH 7.5), and 2 mM $MgCl_2$ at 25°C.

ternary complex, which convert to the distances between Cys 177 of A1 and the active site of 46.9, 47.8, 38.2, and 41.5 Å, respectively. All energy transfer efficiency values were normalized using the value of 29% for S1 (A1) or 13% for S1 (A2) incorporation of BD into SH1 (Cys 707) in the heavy chain. This was done by using observed values of FRET efficiencies between SH1 and the active site (Table I). The corrected energy transfer values (E_{corr}) were computed using the following equation:

$$E_{corr} = (E_{measured} - ratio_{707} \times E_{707})/1 - ratio_{707}$$

where $ratio_{707}$ denotes the ratio of the presence of the donor on Cys 707, and E_{707} denotes the transfer efficiency from Cys 707 to NBD-ATP.

DISCUSSION

The aim of this study was to elucidate the sequential conformational change of the myosin head during ATP hydrolysis that may be directly related to energy transduction, in order to clarify the molecular mechanism underlying the transmission of chemical energy from ATP to the mechanical motility of myosin. We measured FRET between two fluorophores, donor and acceptor, to examine how myosin changes its localized conformation during ATP hydrolysis. We designed a new fluorescent ATP analog, NBD-ATP, to monitor the myosin ATPase cycle, and utilized it for FRET experiments with the fluorescent probes AD and BD. The NBD fluorophore is highly environment-sensitive: although it is moderately fluorescent in aprotic solvents, it is almost nonfluorescent in aqueous solvents. The NBD fluorophore has been demonstrated to be moderately polar, and both its homologous 6- and 12-carbon fatty acid analogs and the phospholipids derived from these probes tend to sense the lipid-water interface region of membranes instead of the hydrophobic interior (*64*). Therefore, NBD-ATP may also sense the hydrophobic region–water interface near the ATPase site. We recently demonstrated that when NBD-ATP binds to myosin, the fluorescence decrease is quenched by 40% (*60*). On the contrary, for kinesin, which has a highly conserved motor domain near the ATPase site, the fluorescence of NBD-ATP is enhanced by about 3-fold (unpublished data). This suggests that the precise conformational difference between the ATPase site in the two motor proteins is reflected by the fluorescence of NBD-ATP.

TABLE I. **Summary of energy transfer measurements between Cys 707 (SHl) or Cys 697 (SH2) labeld with BD and AD and NBD-labeled nucleotides/analogues.** Parameters based on the Förster theory were used as follows: n, the refractive index of the buffer (taken as 1.4); K^2, the orientationfactor assuming free rotation of the donor and acceptor fluorophores (2/3); Q_D, the quantum yield of AD (0.18) and BD (0.12). The efficiencies were derived from the difference spectrum between AD(BD)-S1·NBD-ADP·A1F_4^-(BeF_n) and control of AD(BD)-S1·ADP·A1F_4^-(BeF_n). The fluorescence emission at 515 nm (excited at 390 nm) was used to quanitfy the energy transfer efficiency in different nuleotide states.

Complex	*J* value ($\times 10^{-14}$ $M^{-1}\cdot cm^{-1}$)	R_0 (Å)	FRET efficiency	Distance (Å)	Change in distance (Å)
Cys707 (SHl) → NBD-ATP					
Sl/MgNBD-ADP	5.75 ± 0.02	31.4 ± 0.1	0.332 ± 0.030	35.3 ± 0.8	
Sl/MgNBD-ATP	5.62 ± 0.01	31.3 ± 0.0	0.378 ± 0.032	34.0 ± 0.7	−1.3
S l/MgNBD-ADP/BeF_n	5.60 ± 0.02	31.3 ± 0.0	0.459 ± 0.045	32.2 ± 1.0	−3.1
S1/MgNBD-ADP/AlF_4^-	5.29 ± 0.07	31.0 ± 0.1	0.323 ± 0.046	35.1 ± 1.0	−0.2
Cys697 (SH2) → NBD-ATP					
Sl/MgNBD-ADP	5.82 ± 0.03	34.2 ± 0.0	0,062 ± 0.022	54.0 ± 1.6	
S1/MgNBD-ATP	6.06 ± 0.01	34,4 ± 0.0	0.048 ± 0.015	56.7 ± 1.2	+2.7
S1/MgNBD-ADP/BeF_n	5.89 ± 0.05	34.3 ± 0.1	0.128 ± 0.011	47.2 ± 0.6	−6.8
Sl/MgNBD-ADP/AlF_4^-	5.75 ± 0.04	34.2 ± 0.1	0.074 ± 0.013	52.1 ± 0.9	−1.9

TABLE II. **Summary of FRET measurements between A1 or A2 labeled with BD and NBD-labeled nucleotides/analogues.** The same parameters as in Table I were used. The efficiencies were derived from the difference spectrum between BD-A1(A2)S1·NBD-ADI·$A1F_4^-$(BeF_n) and control of BD-Al(A2)S1·ADP·$A1F_4^-$(BeF_n). The fluorescence emission at 515 nm (excited at 390 nm) was used to quantify the energy transfer efficiency in different nucleotide states.

Complex	*J* value ($\times 10^{-14}$ $M^{-1}\cdot cm^{-1}$)	R_0 (Å)	FRET efficiency	Distance (Å)	Change in distance (Å)
LCA1 → NBD-ATP					
BD-A1S1/MgNBD-ADP	5.05 ± 0.00	30.8 ± 0.0	0.082 ± 0.022	46.1 ± 0.1	
BD-A1S1/MgNBD-ATP	4.91 ± 0.02	30.7 ± 0.1	0.151 ± 0.03 1	41.1 ± 2.7	–5.0
BD-A1S1/MgNBl-ADP/BeF_n	4.91 ± 0.1	30.6 ± 0.0	0.228 ± 0.029	37.6 ± 1.8	–8.5
BD-A1S1/MgNBD-ADP/AlF_4^-	5.06 ± 0.03	30.8 ± 0.1	0.249 ± 0.037	37.1 ± 1.2	–9.0
LCA2 → NBD-ATP					
BD-A2S1/MgNBD-ADP	5.01 ± 0.02	30.7 ± 0.1	0.069 ± 0.029	47.9 ± 10.5	
BD-A2S1/MgNBD-ATP	4.79 ± 0.02	30.5 ± 0.1	0.065 ± 0.041	48.4 ± 0.7	+0.5
BD-A2S1/MgNBD-ADP/BeF_n	4.82 ± 0.03	30.6 ± 0.1	0.212 ± 0.032	39.0 ± 0.9	–8.9
BD-A2S1/MgNBD-ADP/AlF_4^-	5.08 ± 0.04	30.9 ± 0.2	0.124 ± 0.039	42.1 ± 1.1	–5.8

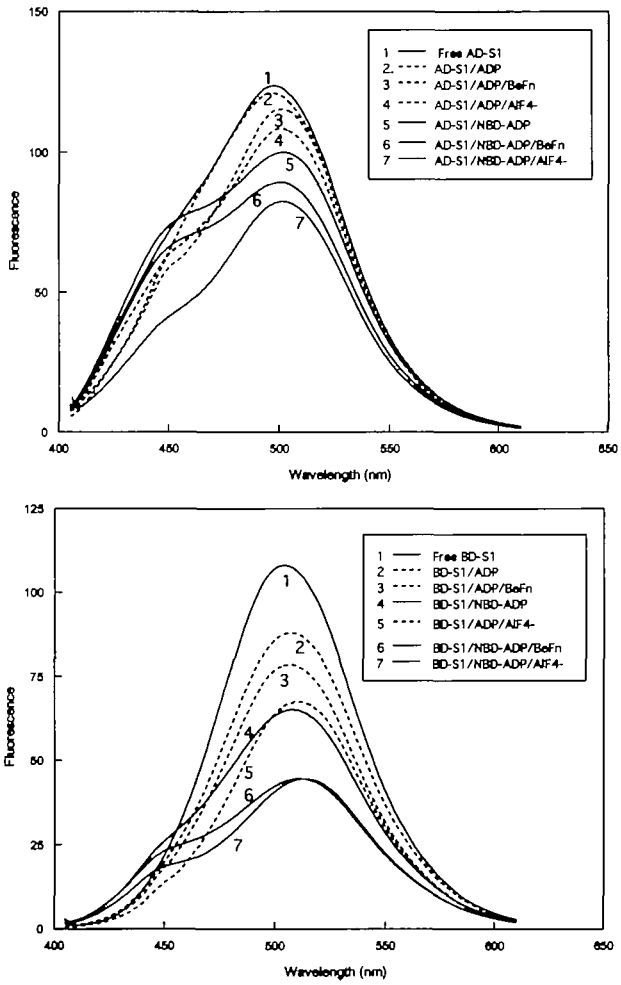

Fig. 10. **Energy transfer from fluorescent probes at SH1 and SH2 to NBD-labeled nucleotides/analogs.** The emission spectra of AD-S1 (A) and BD-S1 (B) (0.6 μM) free in solution were compared with those of NBD-labeled nucleotides/analogs to bound to AD-S1. NBD-ATP (3 μM) was mixed with labeled-S1 (0.6 μM) in 120 mM NaCl, 30 mM Tris-HCl (pH 7.5), and 2 mM $MgCl_2$ at 25°C. After the completion of hydrolysis, ternary complex formation was initiated by the addition of 1 mM BeF_n or 1 mM AlF_4^- and the mixtures were incubated for 3 h in the dark. The emission spectra of labeled-S1 were collected at 405–620 nm with an excitation wavelength of 390 nm. The fluorescence emission at 515 nm (excited at 390 nm) was used to quantify the energy transfer efficiency in different nucleotide states. The dotted lines indicate the control spectra in the absence of acceptor; ADP was used instead of NBD-ADP.

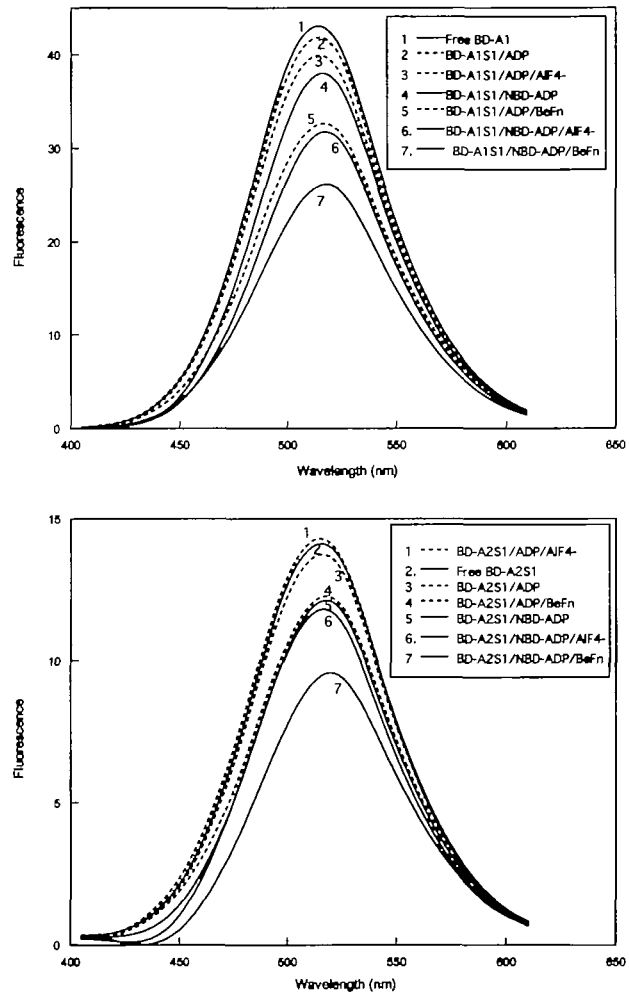

Fig. 11. **FRET between A1 or A2 labeled with BD- and NBD-labeled nucleotides/analogs.** The emission spectrum of BD-A1 (A) or BD-A2 (B) (0.6 μM) free in solution was compared with those of NBD-labeled nucleotides/analogs (3 μM) bound to labeled S1. The emission spectra of labeled S1 were collected at 405–620 nm with an excitation wavelength of 390 nm. The fluorescence emission at 515 nm (excited at 390 nm) was used to quantify the energy transfer efficiency in different nucleotide states. The dotted lines indicate the control spectra in the absence of acceptor; ADP was used instead of NBD-ADP.

We also showed that NBD-ATP is a good substrate for myosin. NBD-ATP is hydrolyzed by myosin in a similar manner to regular ATP in terms of divalent metal dependency, and the myosin ATPase reaction could be monitored from its florescence change. NBD-ATP also supports actin translocation (*60*).

Conformational Changes in the SH1-SH2 Region—It is well established that the reactivity of the sulfhydryl groups on Cys 707 (SH1) and Cys 697 (SH2) is very sensitive to nucleotide binding (*65*). Moreover, these residues can be cross-linked by a variety of bifunctional reagents with different spans (*67–70*), and in the swinging-neck model of muscle contraction, this flexible region has been identified as a fulcrum point (*19, 28, 31*). Based on analysis of the behavior of fluorescent probes, Hiratsuka speculated that the SH1–SH2 region acts as an energy transduction loop through which intersite communication between the ATP and actin binding sites is transmitted and suggested that the sequence of transient intermediates may be reflected in the changing conformation of the SH1–SH2 region (*45, 49, 50*). To precisely detect these localized conformational changes of the SH1–SH2 helix, we measured the energy transfer between SH1 or SH2 and the ATP binding site using specific fluorescent probes. The fluorescent probes AD and BD, which bind specifically to SH2 and SH1, respectively, carry a common fluorophore of the 6-acyl-2-dimethylaminonaphthalene (prodan) group. Hiratsuka has shown that the fluorescence of these probes when bound to SH1 and SH2 is not accessible by ATP binding (*62*). Furthermore, the fluorescence emission spectra of AD and BD overlap well with the excitation spectrum of NBD-ATP (Fig. 8). Therefore, AD and BD are suitable fluorescent probes, and efficient energy transfer from the fluorescence donor, AD and BD, to NBD-ATP, the fluorescence acceptor, is anticipated. The addition of NBD-ATP to AD- and BD-S1 induced a reduction in the fluorescence intensities of AD and BD, and resulted in energy transfer from the donor fluorophore to the acceptor fluorophore (Fig. 10). The relative distance between the active site and SH1 or SH2 was closest in the BD- or AD-S1·NBD-ADP·BeF_n complexes, which mimic the M*·ATP state (Table I). We have also observed a difference in efficiencies between BD- or AD-S1·NBD-ADP·BeF_n and BD- or AD-S1·NBD-ADP·AlF_4^-. The results of the FRET experiments suggest that the SH1 and SH2 region changes its localized conformation to get closer to the ATPase site in the M**·ADP·P_i state than in the M*·ADP state, under physiological solution conditions.

Previous studies have suggested that conformational changes around the SH2 region are induced by nucleotide binding that is not accompanied by conformational changes around SH1 (*62, 70*). The two regions behave independently and exhibit opposite changes in a similar environment. Comparison of the crystal structure of S1·ADP with S1 in the absence of nucleotide and the S1·ADP·AlF_4^- complex has demonstrated that the SH2 helix does not change its conformation in the ATPase cycle. In contrast, the SH1 helix changes dramatically (*70*). The SH1 helix was not observed in the crystal structure of S1·ADP, indicating melting of the helix, whereas the helix was seen in the MgADP·AlF_4^- complex. However, in the present study, the FRET experiments indicated that the SH2 region changes its conformation to get significantly closer than the SH1 region to the ATPase site in the ATPase cycle. It is known that only in the presence of ADP, DTNB induces direct cross-linking of the S-S bond between SH1 and SH2. Therefore, the crystal structure may not represent the physiological structures.

Movement of the Tail Domain of S1 during the ATPase Cycle—Previous X-ray small angle solution scattering and quick-freeze deep etch replica electron microscopic observation studies demonstrated that the myosin head kinks strongly during ATP hydrolysis (*22, 23, 25*). The global conformational change of the myosin head is thought to be associated directly with generating the driving force based on the lever arm theory. However, the precise conformational change of the bending during ATP hydrolysis remains unclear. To study how the myosin head bends along the myosin ATPase kinetic pathway, we measured the FRET between Cys 136 (A2) or Cys 177 (A1) of ELC in the lever arm of the regulatory domain and the active site in the motor domain. Distances from Cys 136 and Cys 177 in ELC to the NBD-fluorophore in the ATPase site were 46.1 and 46.9 Å, respectively, in the MgADP state (Table II). The distances calculated from FRET efficiency were consistent with those seen in the crystal structure when Ser 324 is regarded as the center of the ATPase site. The ribose moiety of the nucleotide corresponds to Ser 324 in the ATP binding pocket of the myosin crystal structure. Our results suggest that the distance from the ELC to the ATPase site is shorter in weak binding states (MgATP and MgADP·P_i) and longer in the strong binding state (MgADP) for both the A1 and A2 isoforms. Previous FRET experiments on rabbit skeletal muscle (*71*) and *D. discoideum* myosin II (*72, 73*) during the MgATPase cycle are consistent with the present results. During the hydrolysis of ATP, Cys 136 and Cys 177 of ELC move closer to the active site by approximately 9 Å. This value is larger than that reported for rabbit skeletal muscle myosin by Smyczynski *et al.* (*71*). However, according to motility assays using single molecule techniques, the step size of myosin is 40–110 Å (*32–34*), which requires a physical swing of at least 60° (*35*). The values for the changes in distance observed in this study are too small to be consistent with the previously reported step size for myosin. Indeed, some previous studies suggested that the conformational change of the light chain binding site was insufficient to explain the bending motion of the lever arm (*71, 73*). However, reorientation of the helix is approximately 30° or less (*74, 75*), which is consistent with our present results (see "RESULTS"). In the S1·ADP·P_i state, if the light chain binding domain bends uniformly along its length rather than rotating as a rigid body, points located in the middle of the helix would move by relatively small distances that may be difficult to detect. This hypothesis is supported by the theoretical calculation that the neck region acts more like an elastic cantilever than a rigid lever as proposed by Spudich *et al.* (*76*).

Warshaw *et al.* (*77*) recently demonstrated that the relationship between the length of the light chain binding site and the step size of myosin is linear. They concluded that changes in the length of the light chain binding domain affect the unitary displacement and force of both shorter- and longer-necked constructs, a finding that is consistent with the neck acting as a mechanical lever arm. An alternative view of the neck has been championed by Yanagida and colleagues (*78*). Although they also observed reduced velocity with a neckless construct of *Dictyostelium* myosin,

they showed that the unitary step size was unaffected by changes in neck length. Therefore, they concluded that the slower velocity was due only to an increase in the time of attachment following the powerstroke. Furthermore, class-V myosin has a long neck domain and proceeds along actin filaments in large steps (36 nm), and a recent study suggested that myosin-V–truncated mutants with neck domains only one-sixth of the native length do not affect the processivity and step distance along actin (*79*). The latter researchers argued that the large step size of myosin V is determined by the motor core domain. Therefore, whether the generation of force is directly induced by motion of the tail domain remains controversial.

In summary, we have demonstrated that a fluorescent ATP analog, NBD-ATP, is applicable to kinetic and topological studies of myosin ATPase using FRET. FRET studies demonstrated that the relative distance between SH1 and SH2 and the ATP binding site is larger in the M^{**}·ATP state than in the M^{**}·ADP state. The change in distance between the ELC binding site and the catalytic domain was too small to be consistent with a simple lever arm model. Investigation of the behavior of the tail domain in the presence of actin may provide further insight into the motility mechanism of myosin.

REFERENCES

1. Mueller, H. and Perry, S.V. (1965) Characterization of the molecular region containing the active sites of myosin. *J. Biol. Chem.* **240**, 3816–3828
2. Cooke, R., Crowder, M.S., Wendt, C.H., Bamett, V.A., and Thomas, D.D. (1984) Muscle cross-bridges: do they rotate? *Adv. Exp. Med. Biol.* **170**, 413–427.
3. Vebert, P. and Cohen, C. (1988) Domains, motions and regulation in the myosin head. *J. Muscle Res. Cell Motil.* **9**, 296–305
4. Werber, M.M., Szent-Gyorgye, A.G., and Fasman, G.D. (1972) Fluorescence studies on heavy meromyosin-substrate interaction. *Biochemistry* **11**, 2872–2883
5. Bagshaw, C.T., Eccelston, J.F., Ekstein, F., Goody, R.S., Gutfreund, H., and Trentham, D.R. (1974) The magnesium ion-dependent adenosine triphosphatase of myosin. Two-step processes of adenosine triphosphate association and adenosine diphosphate dissociation. *Biochem. J.* **141**, 351–364
6. Rosenfeld, S.S. and Taylor, E.W. (1984) Reactions of 1-N6-ethanoadenosine nucleotides with myosin subfragment 1 and actosubfragment 1 of skeletal and smooth muscle. *J. Biol. Chem.* **259**, 11908–11919
7. Woodward, S.K., Geeves, M.A., and Manstein, D.J. (1995) Kinetic characterization of the catalytic domain of Dictyostelium discoideum myosin. *Biochemistry* **34**, 16056–16064
8. Kurzawa, S.E. and Geeves, M.A. (1996) A novel stopped-flow method for measuring the affinity of actin for myosin head fragments using microgram quantities of protein. *J. Muscle Res. Cell Motil.* **17**, 669–676
9. Kurzawa, S.E., Manstein, D.J., and Geeves, M.A. (1997) Dictyostelium discoideum myosin II: characterization of functional myosin motor fragments. *Biochemistry* **36**, 317–323
10. Cremo, C.R. and Geeves, M.A. (1998) Interaction of actin and ADP with the head domain of smooth muscle myosin: implications for strain-dependent ADP release in smooth muscle. *Biochemistry* **37**, 1969–1978
11. Goodno, C.C. (1979) Inhibition of myosin ATPase by vanadate ion. *Proc. Natl. Acad. Sci. USA* **76**, 2620–2624
12. Maruta, S., Henry, G.D., Sykes, B.D., and Ikebe, M. (1993) Formation of the stable myosin-ADP-aluminum fluoride and myosin-ADP-beryllium fluoride complexes and their analysis using ^{19}F NMR. *J. Biol. Chem.* **268**, 7093–7100
13. Werber, M.M., Peyser, Y.M., and Muhlrad, A. (1992) Characterization of stable beryllium fluoride, aluminum fluoride, and vanadate containing myosin subfragment 1-nucleotide complexes. *Biochemistry* **31**, 7190–7197
14. Phan, B. and Reisler, E. (1992) Inhibition of myosin ATPase by beryllium fluoride. *Biochemistry* **31**, 4787–4793
15. Gopal, D. and Burke, M. (1995) Formation of stable inhibitory complexes of myosin subfragment 1 using fluorescandium anions. *J. Biol. Chem.* **270**, 19282–19286
16. Maruta, S., Uyehara, Y., Homma, K., Sugimoto, Y., and Wakabayashi, K. (1999) Formation of the myosin-ADP-gallium fluoride complex and its solution structure by small-angle synchrotron X-ray scattering. *J. Biochem.* **125**, 177–185
17. Maruta, S., Aihara, T., Uyehara, Y., Homma, K., Sugimoto, Y., and Wakabayashi, K. (2000) Solution structure of myosin-ADP-MgF_n ternary complex by fluorescent probes and small-angle synchrotron X-ray scattering. *J. Biochem.* **128**, 687–94
18. Park, S., Ajtai, K., and Burghardt, T.P. (1999) Inhibition of myosin ATPase by metal fluoride complexes. *Biochim. Biophys. Acta* **1430**, 127–140
19. Fisher, A.J., Smith, C.A., Thoden, J.B., Smith, R., Sutoh, K., Holden, H.M., and Rayment, I. (1995) X-ray structures of the myosin motor domain of Dictyostelium discoideum complexed with MgADP-BeFx and MgADP-AlF_4^-. *Biochemistry* **34**, 8960–8972
20. Smith, C.A. and Rayment, I. (1996) X-ray structure of the magnesium (II).ADP.vanadate complex of the Dictyostelium discoideum myosin motor domain to 1.9 Å resolution. *Biochemistry* **35**, 5404–5417
21. Rayment, I., Rypniewski, W.R., Schmidt-Base, K., Smith, R., Tomchick, D.R., Benning, M.M., Winkelmann, D.A., Wasenberg, G., and Holden, H.M. (1993) Three-dimensional structure of myosin subfragment-1: a molecular motor. *Science* **261**, 50–58
22. Katayama, E. (1989) The effects of various nucleotides on the structure of actin-attached myosin subfragment-1 studied by quick-freeze deep-etch electron microscopy. *J. Biochem.* **106**, 751–770
23. Katayama, E. (1998) Quick-freeze deep-etch electron microscopy of the actin-heavy meromyosin complex during the in vitro motility assay. *J. Mol. Biol.* **278**, 349–367
24. Ito. K., Liu. X., Katayama, E., and Uyeda, T.Q.P. (1999) Cooperativity between two heads of dictyostelium myosin II in *in vitro* motility and ATP hydrolysis. *Biophys. J.* **76**, 985–992
25. Wakabayashi, K., Tokunaga, M., Kohno, I., Sugimoto, Y., Hamanaka, T., Takezawa, Y., Wakabayashi, T., and Amemiya, Y. (1992) Small-angle synchrotron x-ray scattering reveals distinct shape changes of the myosin head during hydrolysis of ATP. *Science* **258**, 443–447
26. Lowey, S., Waller, G.S., and Trybus, K.M. (1993) Skeletal muscle myosin light chains are essential for physiological speeds of shortening. *Nature* **365**, 454–456
27. Whittaker, M., Wilson-Kubalek, E.M., Smith, J.E., Faust, L., Milligan, R.A., and Sweeney, H.L. (1995) A 35-Å movement of smooth muscle myosin on ADP release. *Nature* **378**, 748–751
28. Rayment, I. (1996) The structural basis of the myosin ATPase activity. *J. Biol. Chem.* **271**, 15850–15853
29. Uyeda, T.Q.P., Abramson, P.D., and Spudich, J.A. (1996) The neck region of the myosin motor domain acts as a lever arm to generate movement. *Proc. Natl. Acad. Sci. USA* **93**, 4459–4464
30. Dominguez, R., Freyzon, Y., Trybus, K.M., and Cohen, C. (1998) Crystal structure of a vertebrate smooth muscle myosin motor domain and its complex with the essential light chain: visualization of the pre-power stroke state. *Cell* **94**, 559–571
31. Goldman, Y.E. (1998) Wag the tail: structural dynamics of actomyosin. *Cell* **93**, 1–4
32. Molloy, J.E., Burns, J.E., Kendrick-Jones, J., Tregear, R.T., and White, D.C. (1995) Movement and force produced by a single myosin head. *Nature* **378**, 209–212
33. Finer, J.T., Simmons, R.M., and Spudich, J.A. (1994) Single myosin molecule mechanics: piconewton forces and nanometre steps. *Nature* **368**, 113–119
34. Guilford, W.H., Dupuis, D.E., Kennedy, G., Wu, J., Patlak, J.B.,

and Warshaw, D.M. (1997) Smooth muscle and skeletal muscle myosins produce similar unitary forces and displacements in the laser trap. *Biophys. J.* **72**, 1006–1021
35. Holmes, K.C. (1997) The swinging lever-arm hypothesis of muscle contraction. *Curr. Biol.* **7**, R112–R118
36. Jontes, J.D., Wilson-Kubalek, E.M., and Milligan, R.A. (1995) A 32 degree tail swing in brush border myosin I on ADP release. *Nature* **378**, 751–753
37. Kinose, F., Wang, S.X., Kidambi, U.S., Moncman, C.L., and Winkelmann D.A. (1996) Glycine 699 is pivotal for the motor activity of skeletal muscle myosin. *J. Cell. Biol.* **134**, 895–909
38. Gollub, J., Cremo, C.R., and Cooke, R. (1996) ADP release produces a rotation of the neck region of smooth myosin but not skeletal myosin. *Nat. Struct. Biol.* **3**, 796–802
39. Anson, M., Geeves, M.A., Kurzawa, S.E., and Manstein, D.J. (1996) Myosin motors with artificial lever arms. *EMBO J.* **15**, 6069–6074
40. Waller, G.S., Ouyang, G., Swafford, J., Vibert, P., and Lowey, S. (1995) A minimal motor domain from chicken skeletal muscle myosin. *J. Biol. Chem.* **270**, 15348–15352
41. Gollub, J., Cremo, C.R., and Cooke, R. (1999) Phosphorylation regulates the ADP-induced rotation of the light chain domain of smooth muscle myosin. *Biochemistry* **38**, 10107–10118
42. Miller, L., Coppedge, J., and Reisler, E. (1982) The reactive SH1 and SH2 cysteines in myosin subfragment 1 are cross-linked at similar rates with reagents of different length. *Biochem. Biophys. Res. Commun.* **106**, 117–122
43. Tao, T. and Lamkin, M. (1981) Excitation energy transfer studies on the proximity between SH1 and the adenosine triphosphatase site in myosin subfragment 1. *Biochemistry* **20**, 5051–5055
44. Sutoh, K. (1981) Location of SH1 and SH2 along a heavy chain of myosin subfragment 1. *Biochemistry* **20**, 3281–3285
45. Hiratsuka, T. (1988) Cross-linking of three heavy-chain domains of myosin adenosine triphosphatase with a trifunctional alkylating reagent. *Biochemistry* **27**, 4110–4114
46. Ajtai, K. and Burghardt, T.P. (1989) Fluorescent modification and orientation of myosin sulfhydryl 2 in skeletal musde fibers. *Biochemistry* **28**, 2204–2210
47. Rajasekharan, K.N., Mayadevi, M., and Burke, M. (1989) Studies of ligand-induced conformational perturbations in myosin subfragment 1. An examination of the environment about the SH2 and SH1 thiols using a photoprobe. *J. Biol. Chem.* **264**, 10810–10819
48. Kasprzak, A.A., Chaussepied, P., and Morales, M.F. (1989) Location of a contact site between actin and myosin in the three-dimensional structure of the acto-S1 complex. *Biochemistry* **28**, 9230–9238
49. Hiratsuka, T. (1992) Movement of Cys-697 in myosin ATPase associated with ATP hydrolysis. *J. Biol. Chem.* **267**, 14941–14948
50. Hiratsuka, T. (1993) Behavior of Cys-707 (SH1) in myosin associated with ATP hydrolysis revealed with a fluorescent probe linked directly to the sulfur atom. *J. Biol. Chem.* **268**, 24742–24750
51. Xing, J. and Cheung, H.C. (1995) Internal movement in myosin subfragment 1 detected by fluorescence resonance energy transfer. *Biochemistry* **34**, 6475–6487
52. Phan, B.C., Peyser, Y.M., Reisler, E., and Muhlrad, A. (1997) Effect of complexes of ADP and phosphate analogs on the conformation of the Cys707-Cys697 region of myosin subfragment 1. *Eur. J. Biochem.* **243**, 636–642
53. Patterson, B., Ruppel, K.M., Wu, Y., and Spudich, J.A. (1997) Cold-sensitive mutants G680V and G691C of *Dictyostelium* myosin II confer dramatically different biochemical defects. *J. Biol. Chem.* **272**, 27612–27617
54. Lakowics, J.R. (1983) *Principles of Fluorescence Spectroscopy*, pp. 305–309, Plenum Press, New York
55. Miki, M., O'Donoghue, S.I., and DosRemedios, C.G. (1992) Structure of actin observed by fluorescence resonance energy transfer spectroscopy. *J. Muscle Res. Cell Motil.* **13**, 132–145
56. Perry, S.V. (1952) Myosin adenosine triphosphatase. *Methods Enzymol.* **2**, 582–588
57. Weeds, A.G. and Taylor, R.S. (1975) Separation of subfragment-1 isoenzymes from rabbit skeletal muscle myosin. *Nature* **257**, 54–56
58. Robson, R.M., Goll, D.E., and Temple, M.J. (1968) Determination of proteins in "Tris" buffer by the biuret reaction. *Anal. Biochem.* **24**, 339–341
59. Bradford, M.M. (1976) A rapid and sensitive method for the quantitation of microgram quantities of protein utilizing the principle of protein-dye binding. *Anal. Biochem.* **72**, 248–254
60. Maruta, S., Mizukura, Y., and Chaen, S. (2002) Interaction of a new fluorescent ATP analogue with skeletal muscle myosin subfragment-1. *J. Biochem.* **131**, 905–911
61. Youngburg, G.E. and Youngburg, M.V. (1930) A system of blood phosphorus analysis. *J. Lab. Clin. Med.* **16**, 158–166
62. Hiratsuka, T. (1999) ATP-induced opposite changes in the local environments around Cys697 (SH2) and Cys707 (SH1) of the myosin motor domain revealed by the prodan fluorescence. *J. Biol. Chem.* **274**, 29156–29163
63. Prendergast, F.G., Meyer, M., Carlson, G.L., Iida, S., and Potter, J.D. (1983) Synthesis, spectral properties, and use of 6-Acryloyl-2-dimethylaminonaphthalene (Acrylodan). A thiol-selective, polarity-sensitive fluorescent probe. *J. Biol. Chem.* **258**, 7541–7544
64. Chattopadhyay, A. (1990) Chemistry and biological of *N*-(7-nitrobenz-2-oxa-1,3-diazol-4-yl)-labeled lipids: fluorescent probes of biological and model membranes. *Chem. Phys. Lipids* **53**, 1–15
65. Burke, M., Reisler, E., Himmelfarb, S., and Harrington, W.F. (1974) Myosin adenosine triphosphatase. Convergence of activation by actin and by SH1 modification at physiological ionic strength. *J. Biol. Chem.* **249**, 6361–6363
66. Burke, M. and Knight, P.J. (1980) Studies on the role of sulfhydryls in the myosin ATPase. Characterization of the site of modification by the bifunctional sulfhydryl reagent *p*-*N*,*N*'-phenylenedimaleimide. *J. Biol. Chem.* **255**, 8385–8387
67. Miller, L., Coppedge, J., and Reisler, E. (1982) The reactive SH1 and SH2 cysteines in myosin subfragment 1 are cross-linked at similar rates with reagents of different length. *Biochem. Biophys. Res. Commun.* **106**, 117–122
68. Perkins, W.J., Weiel, J., Grammer, J., and Yount, R.G. (1984) Introduction of a donor-acceptor pair by a single protein modification. Forster energy transfer distance measurements from trapped 1,N6-ethenoadenosine diphosphate to chromophoric cross-linking reagents on the critical thiols of myosin subfragment. *J. Biol. Chem.* **259**, 8786–8793
69. Arata, T. (1986) Structure of the actin-myosin complex produced by crosslinking in the presence of ATP. *J. Mol. Biol.* **191**, 107–116.
70. Houdusse, A., Kalabokis, V.N., Himmel, D., Szent-Gyorgyi, A.G., and Cohen, C. (1999) Atomic structure of scallop myosin subfragment S1 complexed with MgADP: a novel conformation of the myosin head. *Cell* **97**, 459–470
71. Smyczynski, C. and Kasprzak, A.A. (1997) Effect of nucleotides and actin on the orientation of the light chain binding domain in myosin subfragment 1. *Biochemistry* **36**, 13201–13207
72. Suzuki, Y., Yasunaga, T., Ohkura, R., Wakabayashi, T., and Sutoh, K. (1998) Swing of the lever arm of a myosin motor at the isomerization and phosphate-release steps. *Nature* **396**, 380–383
73. Xiao, M., Li, H., Snyder, G.E., Cooke, R., Yount, R.G., and Selvin, P.R. (1998) Conformational changes between the active-site and regulatory light chain of myosin as determined by luminescence resonance energy transfer: the effect of nucleotides and actin. *Proc. Natl. Acad. Sci. USA* **95**, 15309–15314
74. Highsmith, S. and Eden, D. (1990) Ligand-induced myosin subfragment 1 global conformational change. *Biochemistry* **29**, 4087–4093
75. Sugimoto, Y., Tokunaga, M., Takezawa, Y., Ikebe, M., and Wakabayashi, K. (1995) Conformational changes of the myosin heads during hydrolysis of ATP as analyzed by x-ray solution scattering. *Biophys. J.* **68**, 29S–34S
76. Howard, J. and Spudich, J.A. (1996) Is the lever arm of myosin

a molecular elastic element? (Appendix to Ref. 29). *Proc. Natl. Acad. Sci. USA* **93**, 4462–4464
77. Warshaw, D.M., Guilford, W.H., Freyzon, Y., Krementsova, E., Palmiter, K.A., Tyska, M.J., Baker, J.E., and Trybus, K.M. (2000) The light chain binding domain of expressed smooth muscle heavy meromyosin acts as a mechanical lever. *J. Biol. Chem.* **275**, 37167–37172
78. Yanagida, T. and Iwane, A.H. (2000) A large step for myosin. *Proc. Natl. Acad. Sci. USA* **97**, 9357–9359
79. Tanaka, H., Homma, K., Iwane, A.H., Katayama, E., Ikebe, R., Saito, J., Yanagida, T., and Ikebe, M. (2002) The motor domain determines the large step of myosin-V. *Nature* **415**, 192–195